

1 **A mathematical model to improve water storage of glacial lakes prediction**
2 **towards addressing glacial lake outburst floods**

3 Miaomiao Qi^{a,b}, Shiyin Liu^{a,b,c*}, Yongpeng Gao^{d,e}, Fuming Xie^{a,b}, Georg Veh^f, Letian Xiao^{a,b},
4 Jinlong Jing^g, Yu Zhu^{a,b}, Kunpeng Wu^{a,b}

5
6 ^a *Yunnan Key Laboratory of International Rivers and Transboundary Eco-Security, 650091 Yunnan*
7 *University, Kunming, China;*

8 ^b *Institute of International Rivers and Eco-Security, Yunnan University, 650091, Kunming, China;*

9 ^c *Yunnan International Joint Laboratory of China-Laos-Bangladesh-Myanmar Natural Resources*
10 *Remote Sensing Monitoring, Kunming 650091, China;*

11 ^d *Faculty of Geography, Yunnan Normal University, Kunming, 650500, China;*

12 ^e *Key Laboratory of Resources and Environmental Remote Sensing for Universities in Yunnan,*
13 *Kunming 650500, China;*

14 ^f *Institute of Environmental Science and Geography, University of Potsdam, Potsdam, Germany*

15 ^g *School of Mathematics and Statistics, Yunnan University, 650091, Kunming, China;*

16
17 *Corresponding author: Shiyin Liu, shiyin.liu@ynu.edu.cn;

18
19 **Abstract:** Moraine-dammed glacial lakes are vital sources of freshwater but also pose a hazard to
20 mountain communities if they drain in sudden glacial lake outburst floods. Accurately measuring
21 the water storage of these lakes is crucial to ensure sustainable use and safeguard mountain
22 communities downstream. However, thousands of glacial lakes still lack a robust estimate of their
23 water storages because bathymetric surveys in remote regions are difficult and expensive. Here we
24 geometrically approximate the shape and depths of moraine-dammed lakes and provide a cost-
25 effective model to improve lake water storage estimation. Our model uses the outline and the terrain
26 surrounding a glacier lake as input data, assuming a parabolic lake bottom and constant hillslope
27 angles. We validate our model using ten new bathymetrically surveyed glacial lakes on the Qinghai-
28 Tibet Plateau, and compiled data from 34 recently measured lakes. Our model overcomes the
29 autocorrelation issue inherent in earlier area/depth-water storage relationships and incorporates an
30 automated calculation process based on the topography and geometrical parameters specific to
31 moraine-dammed lakes. Compared to other models, our model achieved the lowest average relative
32 error of approximately 14% when analyzing 44 observed data, surpassing the >44% average relative
33 error from alternative models. Finally, the model is used to calculate the water storage change of
34 moraine-dammed lakes in the past 30 years in High Mountain Asia. The model has been proven to

35 be robust and can be utilized to update the water storage of lake water for conducting further
36 management of glacial lakes with the potential for outburst floods in the world.

37 **1. Introduction**

38 Moraine-dammed glacial lakes (MDLs) trap meltwater from snow, ice and liquid precipitation
39 within basins behind dams at or near the termini of glaciers (Westoby et al., 2014; Yao et al., 2018;
40 Veh et al., 2019). As glaciers have been retreating in past decades in most mountain regions
41 worldwide, new MDLs have been forming, and existing ones have been growing in size and water
42 storage (Bolch et al., 2012; Carrivick and Tweed, 2013; Cook et al., 2018; Shugar et al., 2020; Zhang
43 et al., 2023). During the period from 1990 to 2018, High Mountain Asia witnessed a remarkable 52%
44 and 54% increase in the number and area of MDLs, respectively (Wang et al., 2020). Notably, the
45 Eastern Himalayas experienced the most significant growth, leading in both the number and area of
46 MDLs during this period. MDLs are vital water reservoirs for communities in glaciated high
47 mountains, but were also repeatedly sources for Glacial Lake Outburst Floods (GLOFs) (Westoby
48 et al., 2014; Wu et al., 2019; Gao et al., 2021; Fischer et al., 2021). According to a report by Lützwow
49 et al. (2023), a total of 630 GLOFs have been linked to MDLs occurring in 27 countries between
50 850 and 2022 CE. A recent study indicates that multiple GLOFs documented from 1964 to 2022
51 have caused damage to infrastructure in High Mountain Asia (Nie et al., 2023).

52 MDLs are prone to sudden failure due to the instability of the dam structure, releasing parts of
53 the impounded water storage in catastrophic floods (Westoby et al., 2014). MDLs can grow towards
54 steep slopes, where debris or ice could fall into the lakes, causing the barriers to overflow (Emmer
55 et al., 2014; Carrivick and Tweed, 2013; Liu et al., 2020). Due to their high altitude and potential
56 energy, these flood waves can attain runout distances of many tens of kilometers, transporting and
57 entraining large amounts of sediments from moraines and riverbanks (Westoby et al., 2014). Many
58 GLOFs have transformed into debris flows and their coarse debris rapidly filled hydropower
59 reservoirs and further destroyed infrastructure along the flow path (Westoby et al., 2014). For
60 example, GLOFs descending from the mountains with high kinetic energy have recently damaged
61 transport and power infrastructure such as the Upper Bhote Koshi hydropower plant, with a
62 reconstruction cost of 57 million USD (United States dollar) (Cook et al., 2018). Future flash floods
63 are a potential threat to major new infrastructure, for example, hundreds more hydropower projects
64 (Nie et al., 2023). GLOFs may also undercut hillslopes along mountain rivers, which may fail,

65 impound river runoff, and form potentially unstable lakes. Thus, MDLs have become a major
66 glacier-related hazard in high mountains, and will likely remain so as glaciers could lose more than
67 a third of their mass by the end of the 21st century (Rounce et al., 2023). Appraising the water
68 storage of glacial lakes is key to allowing for sustainable development along river channels
69 originating in glaciated headwaters (Yao et al., 2018; Harrison et al., 2021; Shugar et al., 2020; Liu
70 et al., 2020).

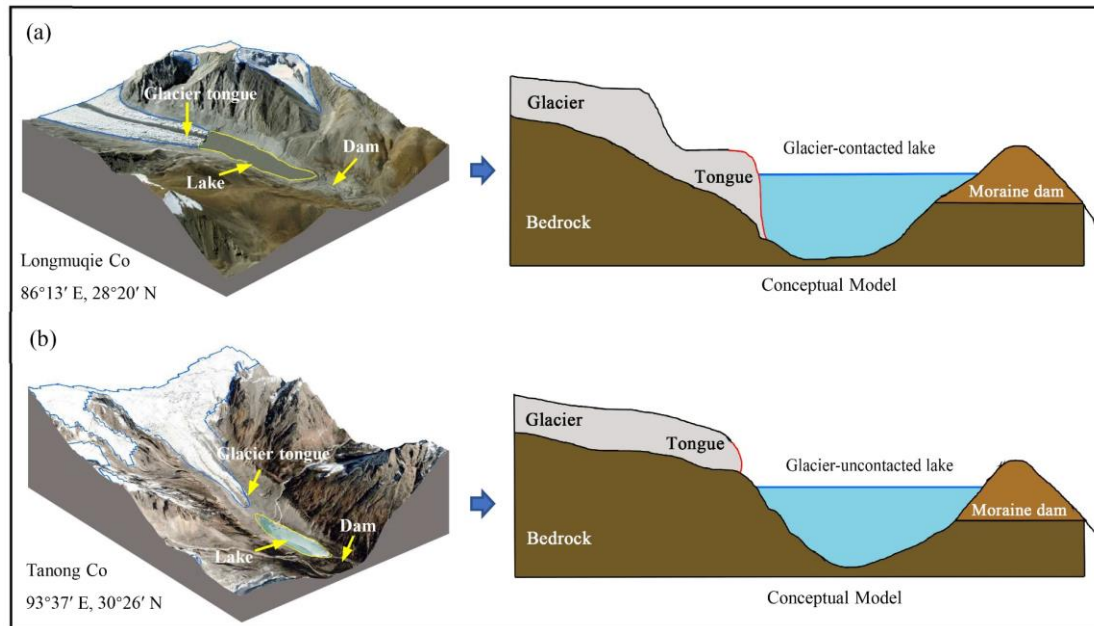
71 The peak discharge during GLOFs is a commonly used parameter for assessing flood hazards
72 and can be derived from empirical formulas related to the lake volume (Clague et al., 2000; Westoby
73 et al., 2014; Sattar et al., 2021; Nie et al., 2023). The failure of the MDLs with the largest water
74 storage has sustained high discharges for many hours, causing widespread inundation in mountain
75 valleys (Mergili et al., 2020). The Sangwang Tsho experienced disastrous outbursts in July 16, 1954,
76 featuring one of the highest reported flood water storages ($71.6 \times 10^6 \text{ m}^3$) and discharges ($\sim 10,000$
77 $\text{m}^3 \cdot \text{s}^{-1}$) (Patel et al., 2017; Veh et al., 2019). Researchers therefore developed numerous empirical
78 regression equations to predict the potential peak discharge during an outburst from a given lake
79 water storage (Wang et al., 2018; Veh et al., 2019; Duan et al., 2023). In any case, these predictions
80 and simulations of peak discharge depend on accurate estimates of lake water storage, ideally
81 obtained through bathymetric surveys. However, measurements of lake depth are expensive and
82 difficult to conduct in high-altitude regions with limited access (Cook and Quincey, 2015; Qi et al.,
83 2022). Therefore, in situ measurements of lake depth are available only for a few dozen cases in the
84 Himalayas, while the water storage remains unknown for the other thousands of lakes in this region.
85 Current optical or radar-based satellite missions, while useful for mapping lakes, are limited in
86 measuring lake bathymetry due to the strong attenuation of electromagnetic waves in glacial lakes
87 (Zhu et al., 2019). As such, there has been an ongoing effort to refine empirical scaling relationships
88 from the few available worldwide samples that relate glacial lake depth and/or area to lake water
89 storage (Fujita et al., 2013; Loriaux and Casassa, 2013; Carrivick and Quincey, 2014; Cook and
90 Quincey, 2015; Veh et al., 2019; Shugar et al., 2020; Qi et al., 2022). However, these equations may
91 yield significant errors in orders of magnitude for a given lake area due to the the autocorrelation
92 issue inherent in earlier area/depth-volume relationships. Although there are models considering the
93 specific geometric shapes and topography surrounding lakes, they limited to estimating the water
94 storage of larger size plateau tectonic lake (Zhou et al., 2020; Zhu et al., 2019). After numerous

95 experiments, we have found that the aforementioned models do not apply to estimating the water
96 storage of glacier lakes due to the lack of consideration for glacial lake and related parameters.
97 Given the critical role of glacial lake water storage in assessing hazard risk and providing early
98 warning information, the development of a mathematically robust yet cost-effective model is
99 urgently needed.

100 Our goal is to introduce a novel approach for accurately estimating water storage by
101 incorporating its geometry and surrounding terrain. To this end, we propose a three-dimensional
102 model to approximate the basin morphology of MDLs and derive its analytical equation. We assess
103 the performance of this model against field-measured underwater topography data and further
104 compare the model error against other available empirical scaling relationships. Finally, we discuss
105 the uncertainty and rationality of the new model and apply the model to estimate the water storage
106 of the MDLs in High Mountain Asia.

107 **2. MDLs types and their geometric approximation**

108 MDLs can be classified into glacier-contacted lakes (GCL) and glacier-uncontacted lakes
109 (GUL). GCLs are supraglacial ponds on top of debris-covered glaciers or lakes at the termini of
110 glaciers (Richardson 2000; Bennett et al., 2012). We term GCL as MDL in direct contact with the
111 glacier terminus (Figure 1a). By contrast, GULs are separated from the present glaciers, but
112 impound substantial parts of the meltwater from the glacier upstream (Figure 1b). The bottom of an
113 MDL may be a sediment-covered bedrock depression that was eroded and deepened by the parent
114 glacier during earlier advances. As glaciers retreat, they provide space for lakes to grow between
115 the glacier terminus, with the abandoned moraine trapping excess meltwater from the parent glacier
116 (Nie et al., 2023).



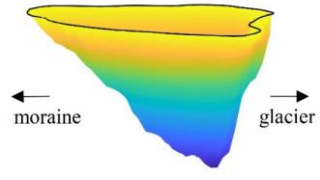
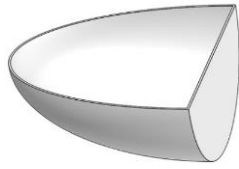
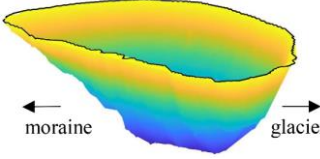
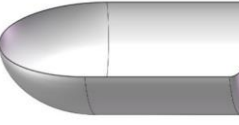
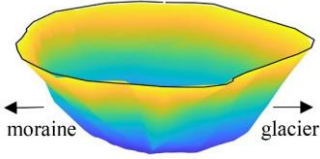

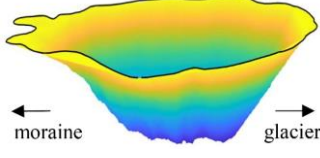
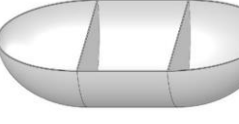
117

118 **Figure 1.** Longitudinal cross-sections along a glacier-contacted (a) and glacier-uncontacted lake (b) (The base
 119 images are from Google Earth imagery) (©Google Earth). Sketches are idealized and do not represent measured
 120 elevations.

121 We use the glacial lake inventory of High Mountain Asia by Wang et al. (2020) to differentiate
 122 these two types of MDLs. In general, glacial lakes grow in area largely because they become longer.
 123 Lower values of the ratio (R) between the maximum width and maximum length indicate that the
 124 shape of the lake is elongated; R equals 1 if the lake is perfectly circular or square (Qi et al., 2022).
 125 According to the glacial lake inventory, the R value for glacial lakes in High Mountain Asia ranges
 126 from 0.1 to 1.0. If R is less than 0.1, it may indicate the presence of glacial lakes with lengths
 127 exceeding 10 meters but widths of approximately 1 meter. However, in reality, glacial lakes with
 128 such dimensions are practically non-existent. Therefore, thresholds of R allow us to distinguish
 129 glacial lakes into four subclasses (Table 1). We find that newly formed GCLs typically have small
 130 surface areas and high values of R . We classified GCLs with R between 0.70 ~ 1.0 as GCL-1, and
 131 those with R less than 0.69 as GCL-2. Examples of these two types are Poiqu No.1 Lake (85.92°E,
 132 28.14°N) and Bienong Co (93°26'E, 30°31'N) (Table 1). With ongoing glacier recession, lakes
 133 might become decoupled from their parent glacier, switching from a lake-terminating to a land-
 134 terminating glacier. We termed lakes as GUL-1, if R ranged between 0.5 and 1.0, and GUL-2 if R <
 135 0.49. Paqu Co (86°15'E, 28°30'N) and Jialong Co in 2020 are the examples of these two classes
 136 (Table 1). It is noteworthy that the establishment of the R threshold in this study is grounded in the
 137 glacial lake catalog dataset developed by Wang et al, (2020). Initially, the glacial lakes were divided

138 into two major categories, GCL and GUL. Subsequently, R values for each glacial lake were
 139 calculated, and all co-authors classified the geometric shapes based on different types and sizes of
 140 glacial lakes. Ultimately, through statistical analysis of glacial lake sizes for different types, we
 141 defined the threshold for R . This allows the model to automatically categorize glacial lakes based
 142 on this value.

143 **Table 1** Examples of glacier-contacted lake and glacier-uncontacted lake. The ratio R represents the maximum width
 144 (m) divided by the maximum length (m) of the glacial lake. The vertical scale is exaggerated.

Type	Lake bathymetry	Model	Features	R
GCL-1	PoiquNo.1 of 2021 		A newly formed MDL typically has a small scale and is located at the glacier tongue.	$0.70 \leq R \leq 1.0$
GCL-2	Bienong Co of 2021 		The MDL gradually grows in the area but has not yet reached the maximum range determined by the surrounding terrain.	$0.10 \leq R \leq 0.69$
GUL-1	Paqu Co of 2020 		As the glacier continues to retreat, the distance between the glacier tongue and the MDL gradually increases.	$0.50 \leq R \leq 1.0$
GUL-2	Jialong Co of 2020 		The length of the MDL increases with time due to the continuous supply with glacier meltwater.	$0.10 \leq R \leq 0.49$

145

146 3. Model Development

147 3.1. Input data

148 We suggest specific geometric models for the four subclasses (Table 1) to approximate the
 149 water storages of MDLs. Our models are fed with data from a digital elevation model (DEM) and
 150 from the outline of a glacial lake. We used a 12.5-meter ALOS PALSAR DEM, which is freely

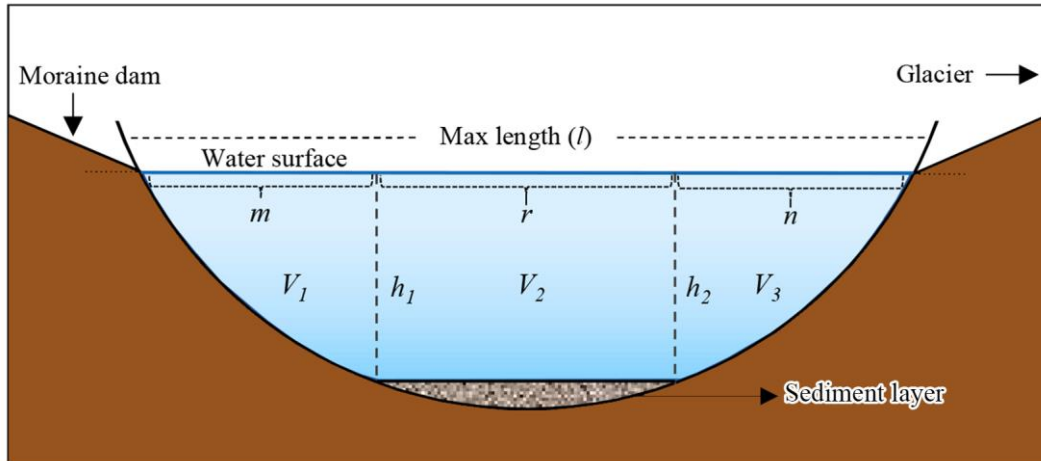
151 available from the Japan Aerospace Exploration Agency (JAXA, <https://www.eorc.jaxa.jp>).

152 3.2. Analytical equations

153 We surmise that an ideal cross-section of a MDL (Figure 2) can be partitioned into three distinct
154 portions, V_1 , V_2 , and V_3 , representing the water storage of the lake stored adjacent to the moraine
155 dam, at the center of the lake, and near the glacier (or bedrock if the lake is disconnected from the
156 glacier). The corresponding lengths of these three portions along the maximum length of the lake
157 are denoted by m , r , and n . The lake has its maximum depth, h_1 and h_2 , on either side of r . Points g
158 and f represent the positions of a sediment layer at the lake bottom, and a and β are the slopes of
159 near the water surface.

160 The core assumptions of our geometric model can be summarized such that: 1) an MDL has a
161 parabolic longitudinal bottom profile with a uniform sediment layer at the bottom of the lake to keep
162 $h_1 = h_2$, and a parabolic cross-section P_S (Figs. 2; 3); (2) the lake surface shape can be approximated
163 by ellipses at both ends and a rectangle in between; (3) The glacier surface and the moraine dam dip
164 towards the lake with the same slope.

165

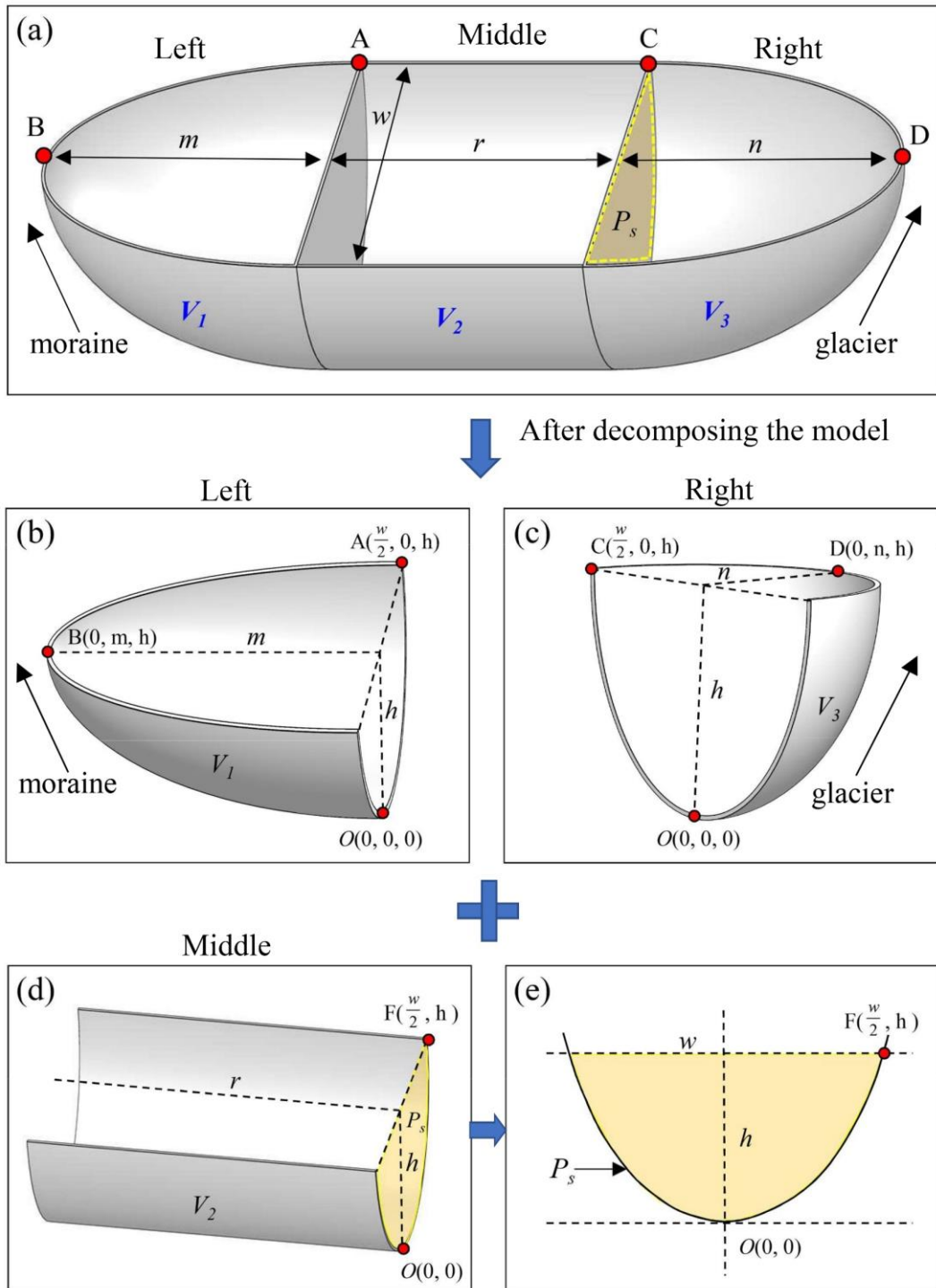


166

167 **Figure 2.** Longitudinal cross-section through a MDL. The blue horizontal line (l) is the maximum length on the lake
168 surface, subdivided by m , r , and n . The solid black line is the hypothetical bottom of the lake, and the gray texture
169 area represents a sediment layer covering the lake bottom. The maximum water depth is $h=h_1=h_2$, and points g and
170 f are at equal depths.

171 In three-dimensional form, the MDL basin can be divided into three parts with each having a
172 water storage of V_1 , V_2 , and V_3 (Figure 3a). V_1 and V_3 can be considered as the water storages of
173 elliptical semi-paraboloids controlled by the water depth h (Figure 3b and c). Significantly, V_1 and
174 V_3 may or may not be equal, depending on the values of m and n . V_2 is a semi-parabolic cylinder

175 (Figure 3d) that has height r , diameter w , and a parabolic cross-section P_s (Figure 3e). Thus, the total
 176 water storage of the MDL is $V=V_1+V_2+V_3$.



177
 178 **Figure 3.** Definition diagram for the geometry of a MDL. a, hypothetical three-dimensional model of a
 179 MDL. b, Model for V_1 describing the lake water storage adjacent to the moraine dam. c, Model for V_1
 180 describing the lake water storage adjacent to the glacier. d, Model for V_3 describing the lake water storage
 181 stored in the center part of the lake. e, Cross section of the column P_s . The parameters m and n are the
 182 semi-major axis of the elliptical paraboloid near the MDL inlet and outlet, respectively; r is the length of
 183 the parabolic cylinder in the middle of MDL; w and l represent the largest width and length of the MDL,

184 respectively; h is the lake depth.

185 To obtain the individual lake water storages, we define the elliptical paraboloids for V_1 and V_2
186 (equations 1-2) in a Cartesian coordinate system (x, y, z) as

$$187 \quad V_1 = \left\{ (x, y, z) \mid \frac{x^2}{a_1^2} + \frac{y^2}{b_1^2} \leq z, y \geq 0, 0 \leq z \leq h \right\} \quad (1)$$

$$188 \quad V_3 = \left\{ (x, y, z) \mid \frac{x^2}{a_2^2} + \frac{y^2}{b_2^2} \leq z, y \geq 0, 0 \leq z \leq h \right\} \quad (2)$$

189 and the parabolic cylinder for V_2 (equation 3) as

$$190 \quad V_2 = \left\{ (x, y, z) \mid kx^2 \leq z \leq h, 0 \leq y \leq r \right\} \quad (3)$$

191 where $a_1 > 0, b_1 > 0, a_2 > 0, b_2 > 0$ are length of the semi-axes of upper surfaces of V_1 and V_3 ; $h >$
192 0 is the height of V_1, V_2 and V_3 ; $r > 0$ is the length of V_2 .

193 Considering the four types of MDLs, GCL-1 corresponds to the case where $r=0$ and $n=0$. In
194 this study, m represents the part of the lake area closer to the moraine dam, and in most cases, m is
195 not equal to zero. However, in certain special cases, such as the Lake Zhasuo Co (93.25°E, 30.31°N)
196 in southeastern Tibet, $m=n=0$, because the surface morphology of this lake is rectangular. In most
197 scenarios, the water storage of the GCL-1 can be represented as:

$$198 \quad V_{\text{GCL1}} = \frac{\pi w m h}{8}. \quad (4)$$

199 When $n=0$, the model of MDL corresponds to GCL-2, and its water storage can be
200 represented as

$$201 \quad V_{\text{GCL2}} = \frac{\pi w m h}{8} + \frac{2}{3} w h r. \quad (5)$$

202 When $r=0$, the model of MDL conforms to GUL-1, and its water storage can be expressed as:

$$203 \quad V_{\text{GUL1}} = \frac{\pi w h l}{4}. \quad (6)$$

204 When the type of MDL corresponds to GUL-2, its water storage can be expressed as:

$$205 \quad V_{\text{GUL2}} = \frac{\pi w h (l - r)}{4} + \frac{2}{3} w h r. \quad (7)$$

206 Finally, the water depth (h) can be derived from the w and slope angles (α) of the glacial lake:

$$207 \quad h = \frac{w \tan(\alpha)}{4}. \quad (8)$$

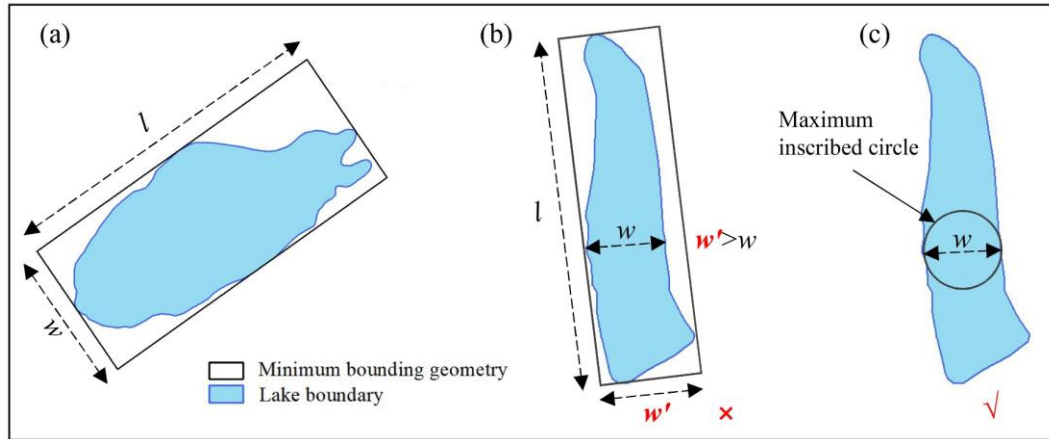
208 Section 1 in the Supplementary file elaborates more on the derivation of these analytical
209 equations, Table 2 shows the definition of the abbreviations in the model procedure.

Table 2. The definition of the abbreviations in the geometric model.

Abbreviation	Description and definition
MDL	The moraine-dammed lake
GUL	The glacier-uncontacted lake
GCL	The glacier-contacted lake
R	The ratio of the maximum width to the maximum length of the MDL
m	The semi-major axis of the elliptical paraboloid of the MDL outlet
n	The semi-major axis of the elliptical paraboloid at the MDL inlet
c	The arbitrary height of the cross-section of an elliptic paraboloid
r	The length of the parabolic cylinder in the middle of MDL
h	The maximum water depth of MDL
w	The diameter of the largest inscribed circle of the MDL
l	The length of the minimum bounding rectangle of MDL
P_s	The cross-section of the middle of MDL
S_{P_s}	The area of the cross-section in the middle of MDL
a	The median slope of the 80 m buffer zone around the MDL

211 3.3. Determination of model parameters

212 We determined the parameters in Eq. 4 - 8, namely w , l , a , m , n and r , using the lake boundary
213 and the DEM. We measured w and l by drawing a minimum rectangle bounding box with length l
214 encompassing the MDL (Figure 4a). If the width w' of the bounding box of the MDL exceeds the
215 actual width (w) of the lake, as in the case of the tortuous boundary of Lake Longmuqie Co (86.23°E,
216 28.35°N) (Figure 4b), we assign the diameter of the maximum inscribed circle within the MDL as
217 w in Figure 4c.



218

219 **Figure 4** Schematic illustration of the method for extracting the maximum length (l) and width (w) of the MDL. The
 220 outline in Figure a represents the geometric boundary of Lake Jialong Co (86.85°E, 28.21°N), while the outlines in
 221 Figures b and c depict the geometric boundaries of Lake Longmuqie Co (86.23°E, 28.35°N).

222 To determine the slope a -value surrounding the MDL, we use a DEM with a spatial resolution
 223 of 12.5 m in the model computation. We tested buffer sizes of 30 m, 50 m, 80 m, and 100 m width
 224 beyond the MDL boundary, and extracted the mean and median value of a within each buffer. By
 225 comparing the simulated results with the measured data, we found that the water storage estimation
 226 using the median value of a within 80 m external buffer zone had a lower relative error and higher
 227 overall accuracy. Therefore, we defined a -value as the median slope within the 80 m buffer zone
 228 surrounding the MDL boundary. The choice of buffer zone distance can be adjusted based on the
 229 specific terrain characteristics of the research area, allowing researchers to adapt the methodology
 230 to their data accuracy.

231 Determining the appropriate thresholds for m , n , and r of different MDL types is challenging
 232 as methods for extracting these parameters vary depending on the MDL types. In other words, due
 233 to the different types of glacial lakes, the values of m , n , and r vary. Additionally, these values change
 234 with the size of the glacial lake. To enable the model to automatically identify and calculate the
 235 corresponding m , n , and r for each glacial lake, we need to define a threshold. Based on the geometry
 236 of the glacial lake, we established a proportional relationship between m , n , r , and the glacier lake
 237 length (l). This proportional relationship is empirically defined and essentially represents a
 238 geometric segmentation of the glacial lake. The lake is divided into three sections, and the volume
 239 of each section is calculated separately. The total water storage of the lake is then obtained by
 240 summing the volumes of these three sections. Relying on R , lake boundary from Wang et al. (2020)

241 as well as DEM, m and n were estimated for GUL-1 and GUL-2 as shown in Table 3. In the case of
 242 GCL-1, $l = m$ due to its small area of water surface. For GCL-2, m was determined as 35% of l for
 243 lakes with $0.50 < R < 0.69$, 30% of l for lakes with $0.30 < R < 0.49$ and 20% of l for lakes with $R < 0.30$
 244 (Table 3).

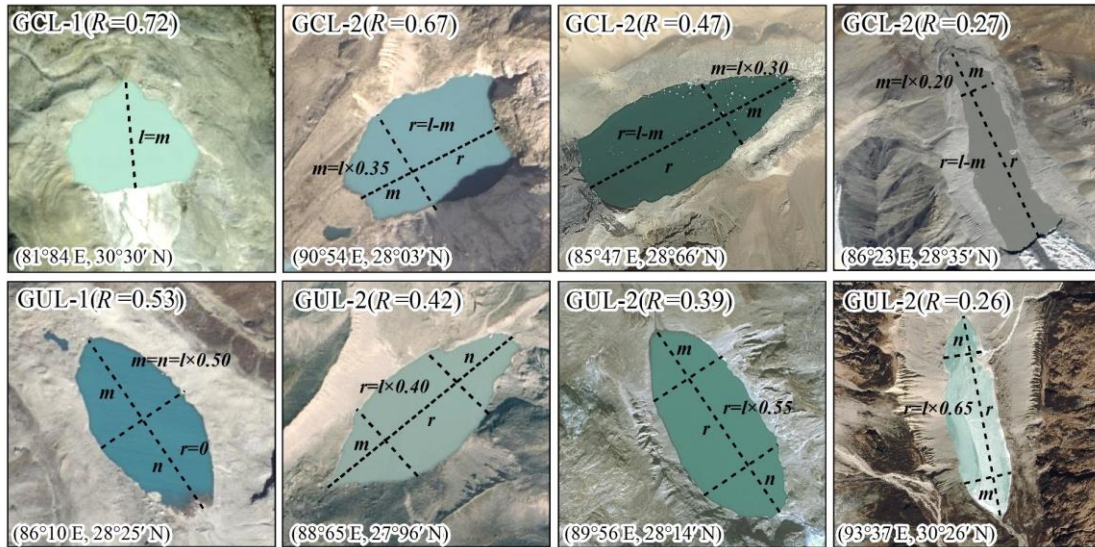
245 For GUL-1, R ranges from 0.50 to 1.0, both m and n are considered equal to half of l . On the
 246 other hand, for GUL-2, it is possible to estimate the MDL water storage solely based on r , as
 247 described in Equation 7. Accordingly, r values were statistically set up as $0.4l$, $0.55l$, and $0.65l$,
 248 respectively with three R levels (Table 3). Figure 5 illustrates several representative cases of MDLs.

249 The above quantitative question about m , n and r is not based on subjective judgment. First,
 250 we computed the R values for all glacial lakes utilizing catalog data, then categorized them by glacial
 251 lake type, and finally, we provided a definition by statistically assessing the shape of glacial lakes.
 252 This definition pertains to the proportionality of m , n , and r concerning the l of the glacial lake.
 253 Consequently, our model is capable of autonomously classifying each glacial lake type through
 254 boundary data analysis. It further computes various parameters for each lake, encompassing m , n , r ,
 255 and h , ultimately culminating in the determination of the water storage for each lake.

256 **Table 3** Quantification of model input parameters.

Lake type	Calculation rules of model input parameters					
	a	w, l	R	m	n	r
GCL-1			$0.70 \leq R \leq 1.0$	l	0	0
			$0.50 \leq R \leq 0.69$	$l \times 0.35$	0	$l - m$
GCL-2	Median slope within the 80 m buffer zone outside the lake boundary	w is the diameter of the largest inscribed circle and l is the maximum length of the minimum bounding geometry	$0.30 \leq R \leq 0.49$	$l \times 0.30$	0	$l - m$
			$0.10 \leq R \leq 0.29$	$l \times 0.20$	0	$l - m$
GUL-1			$0.50 \leq R \leq 1.0$	$l \times 0.50$	$l \times 0.50$	0
			$0.40 \leq R \leq 0.49$			$l \times 0.40$
GUL-2			$0.30 \leq R \leq 0.39$	$l - r$		$l \times 0.55$
			$0.10 \leq R \leq 0.29$			$l \times 0.65$

257

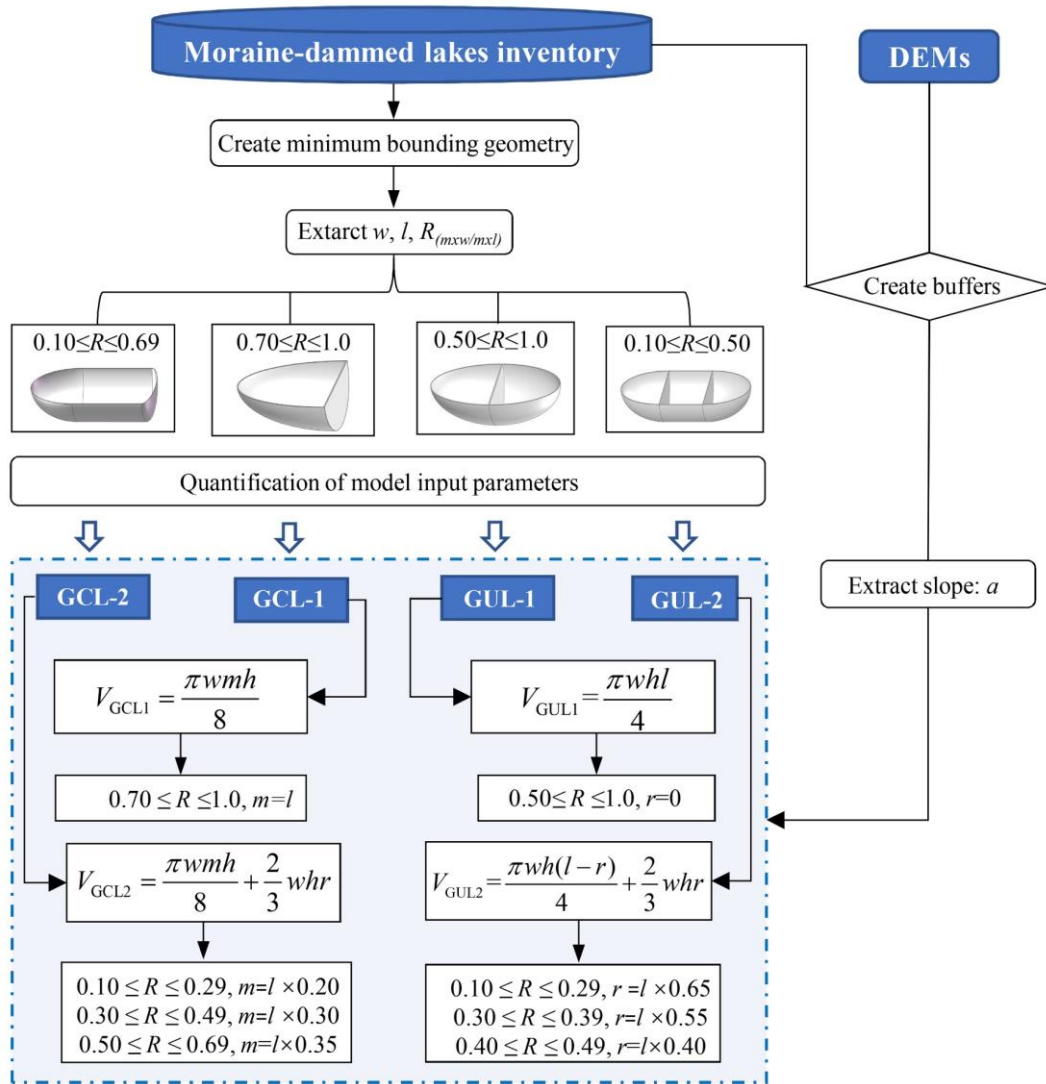


258

259 **Figure 5.** Example for the extraction of input parameters for different types of MDLs. The base map is a Google
 260 Earth image (©Google Earth).

261 We executed our workflow (Figure 6) on 44 MDLs in High Mountain Asia that have known
 262 depths and water storages. For each lake, we checked whether its outline was in contact to the parent
 263 glacier. We automatically fitted a rectangular bounding box to calculate R , and then automatically
 264 assigned each lake to one of the four types of MDL based on R thresholds (Table 1). Finally, we
 265 estimated their water storages using our and traditional empirical relationships. Our model requires
 266 MDL boundary and DEM data as inputs, and it automatically quantifies each parameter while
 267 selecting the optimal model for water storage estimation.

268 Finally, we applied our model to more than 10,000 glacial lakes with unknown bathymetry in
 269 High Mountain Asia. This region had one of the highest rates of MDLs growth in the world in past
 270 decades.



271

272 **Figure 6.** The flow chart of the model procedure derivation.

273 3.4. Model validation and application

274 In this study, we initially validated our parameterization using bathymetric measurements from
 275 four representative glacial lakes surveyed between 2020 and 2021. Subsequently, we combined the
 276 data from these four lakes with the remaining six glacier lakes we measured, along with water
 277 storage data from 34 MDLs obtained from relevant literature sources (see Appendix A for details).
 278 This resulted in a dataset of 44 lakes, which was used to compare and validate the performance of
 279 our model against other existing methods.

280 A glacier lake inventory of the High Mountain Asia region, published by Wang et al, 2020 was
 281 used as input data for the model application to assess the water storage of moraine-dammed lakes
 282 in this region. Notably, Wang's glacier lake inventory provides a detailed classification of GCL and
 283 GUL, which has been internationally recognized. It is important to note that in his dataset, GUL

284 refers specifically to glacier lakes that do not contact glaciers, which may not necessarily all be
285 moraine-dammed lakes. We conducted a thorough review and made revision to ensure that we
286 retained only those GULs classified as moraine-dammed lake.

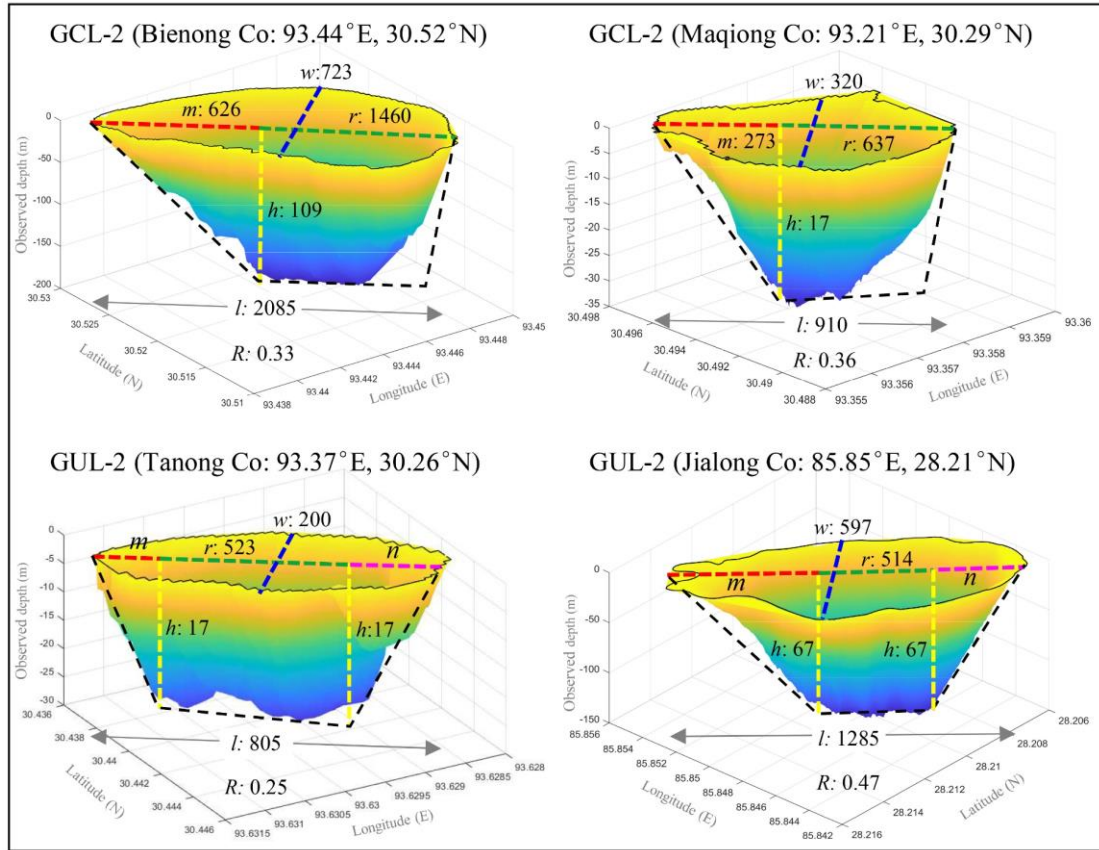
287 **4. Results**

288 **4.1. Model validation**

289 We validated our parameterization using bathymetry measurements from four representative
290 glacial lakes, namely, Bienong Co, Maqiong Co, Tanong Co, and Jialong Co, located in the Qinghai-
291 Tibet Plateau. These lakes represent the four types of glacier lakes, with depths measured through
292 bathymetric surveying (Figure 7). In comparing estimated with measured water storages (Table 4),
293 we find that Jialong Co has the highest accuracy with a relative error of only 1%. Maqiong Co and
294 Tanong Co are overestimated by approximately 5% and 7%, respectively. The largest lake, Bienong
295 Co, had an underestimated water storage of 6%.

296 In addition, our model is designed to approximate the mean depth of MDLs and therefore
297 underestimates the maximum measured lake depth by about 50% (Table 4). Modeled mean water
298 depths only deviate by 18% (mean) from the measured mean water depths. Except for a notable
299 prediction error for Bienong Co (+47%), errors for Jialong Co, Tanong Co, and Maqiong Co range
300 from 6% to 13% relative to the measured values.

301 In summary, our model has a high degree of concordance with observed glacial lake water
302 storages and provides better estimations of water depth compared to the measured average depths.
303 This suggests that our proposed model can be used in glacial lake water storage estimation and the
304 management of GLOF hazards.



305

306 **Figure 7.** Subaqueous glacial lake morphology based on bathymetric surveys. The black dashed line represents the
 307 hypothetical longitudinal profile of the glacial lake; l and w are measured from the lake boundary, h is simulated
 308 lake depth and the remaining parameters (m , n , r) are calculated by rule in Table 3. Lake depth is exaggerated.

309 **Table 4** Validation results of the mathematical model.

Name	Year of survey	Type	Area (km ²)	Lake depth (m)			Water storage (10 ⁶ m ³)		
				Observed (max/mean)	Simulated (mean)	Relative error	Observed	Simulated	Error
Bienong Co	2021	GCL2	1.16	181/74	109	+47%	102.00	95.689	-6%
Maqiong Co	2021	GCL2	0.22	34/16	17	+6%	3.325	3.581	+7%
Tanong Co	2021	GUL2	0.13	29/15	17	+13%	1.821	1.915	+5%
Jialong Co	2020	GUL2	0.55	135/62	67	+8%	37.530	37.952	+1%

310

311 4.2. Comparison with other methods

312 Table 5 displays the dataset of glacial lake bathymetry used in this study to validate the model.
 313 We compared our model with another model that employed the lake geometry (Zhou et al., 2020),
 314 and also with 20 additional formulas (EqS1-EqS20) collated by Qi et al. (2022) in Table S1. In the
 315 estimation of a single MDL, formulas EqS4, EqS6, EqS13, EqS17, and EqS20 displayed significant
 316 inaccuracies (132% - 853%). For instance, EqS13 shows an average error of 853%. Consequently,

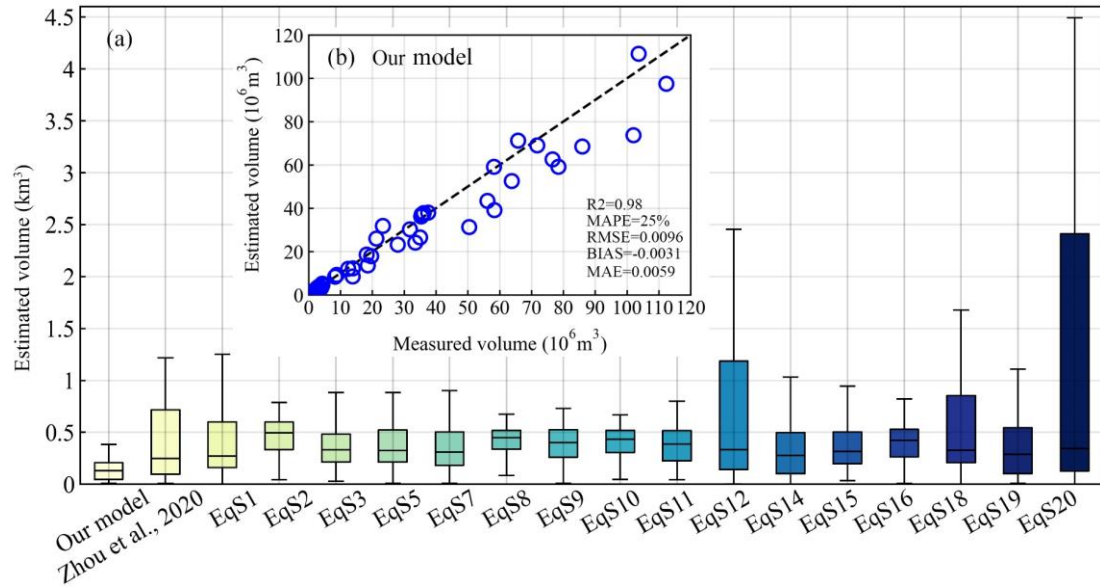
317 we have refrained from conducting a comparative analysis of these five formulas in the subsequent
 318 discussions.

319 **Table 5** The glacial lake bathymetry data set used in this study. The lake bathymetry data are shown in bold provided
 320 by this study, and the rest are obtained from references, see Appendix A for details.

Lake Name	Type	Area (km ²)	Water storage(10 ⁶ m ³)		Measurements based on remote sensing images						
			Measured	Estimated	<i>l</i>	<i>w</i>	<i>R</i>	<i>a</i>	<i>m</i>	<i>r</i>	<i>h</i>
Kajiaqu	GCL2	0.29	3.45	3.00	1436	230	0.13	14	287	1149	15
Bienong Co	GCL2	1.17	102.00	95.69	2085	723	0.33	31	626	1460	109
Longmuqie Co	GCL2	0.58	8.28	8.47	1775	380	0.21	12	355	1420	21
Tanong Co	GUL2	0.13	1.82	1.92	805	200	0.25	19	0	523	17
Maqiong Co	GCL2	0.22	3.32	3.58	910	320	0.36	12	273	673	17
Zhasuo Co	GUL2	0.33	4.28	5.18	890	380	0.4	12	0	356	21
Jialong Co	GUL2	0.55	37.53	37.95	1285	597	0.46	24	0	514	67
Paqu Co	GUL2	0.58	8.80	9.22	2134	314	0.15	14	0	1387	19
Chmaqudan Co	GUL2	0.56	19.61	17.91	1459	450	0.31	19	0	802	38
Tara Co	GUL2	0.23	2.64	3.19	1024	255	0.26	15	0	666	17
Jialong Co	GUL2	0.46	18.20	18.59	1133	537	0.47	17	0	453	41
Rewuco	GCL1	0.42	13.85	8.52	839	613	0.73	15	839	0	42
PoiqNo.1	GCL2	0.09	2.53	2.21	428	300	0.64	22	150	278	30
Ranzeria Co	GCL2	0.29	3.88	3.16	1181	288	0.23	12	236	945	15
BethungTsho	GCL2	0.45	4.28	4.51	1355	373	0.28	9	271	1084	15
Guangxie Co	GCL2	0.41	2.61	2.71	1032	390	0.3	7	310	722	12
Shishapangma	GCL2	0.6	18.59	13.61	1721	500	0.29	12	344	1377	26
Lugge	GCL2	1.63	71.76	69.02	3163	578	0.18	23	633	2531	62
Raphstreng2	GCL2	1.31	58.19	59.13	2117	816	0.39	16	635	1482	59
Galong Co	GCL2	5.49	377.39	403.18	4284	1500	0.35	16	1285	2999	107
Bnecuoguo Co	GUL1	0.11	1.69	1.98	490	288	0.59	14	0	0	18
Cirenma Co	GUL2	0.33	12.43	12.03	1276	367	0.29	22	0	829	36
Longbasaba	GCL2	1.15	56.16	43.47	2114	680	0.3	17	634	1479	52
Midui	GCL2	0.22	1.13	1.34	968	280	0.31	7	290	678	8
Lugge	GCL2	1.18	58.30	39.18	2520	545	0.2	19	504	2016	47
Thulagi	GCL2	0.76	31.80	30.33	1991	437	0.22	28	398	1593	57
Tsho Rolpa	GCL2	1.39	76.60	62.59	2942	590	0.2	22	588	2353	59
Imja Tsho	GCL2	0.6	28.00	23.18	1341	543	0.38	22	402	939	54
Cirenma Co	GUL2	0.33	13.90	12.23	1276	370	0.29	22	0	829	37
Pidahu	GCL2	0.89	50.44	31.37	2071	500	0.21	22	414	1657	50
Imja Tsho	GCL2	1.14	63.80	52.55	2191	605	0.24	23	438	1753	65
South Lhonak	GCL2	1.31	65.80	71.22	2328	715	0.31	22	699	1630	73
Tam Pokhari	GCL2	0.45	21.25	26.02	1178	470	0.41	34	353	825	80
Thulagi	GCL2	0.91	23.30	31.83	2522	417	0.17	25	504	2017	49
Imja Tsho	GCL2	1.03	35.50	37.03	2028	556	0.27	21	406	1622	54
Thulagi	GCL2	0.94	35.37	36.19	2541	430	0.17	27	508	2033	54

Tsho Rolpa	GCL2	1.54	85.94	68.58	3304	566	0.17	23	661	2643	60
Thulagi	GCL2	0.92	36.10	37.75	2504	439	0.18	27	501	2003	56
Lower Barun	GCL2	2.14	103.60	111.38	3297	730	0.22	23	659	2638	76
Lower Barun	GCL2	1.77	112.30	97.45	3091	717	0.23	22	618	2473	72
Imja Tsho	GCL2	1.15	78.40	59.12	2208	610	0.24	25	442	1767	72
Amphulapche	GUL1	0.12	3.20	3.79	404	369	0.99	19	0	0	32
Chamlang Tsho	GCL2	0.76	35.00	26.53	1627	588	0.32	18	488	1139	47
Imja Tsho	GCL2	0.75	33.48	24.13	1557	550	0.32	19	467	1090	48

321 Our assessment (Table 6) involves the relative error (RE, absolute value), bias, root mean
322 square error (RMSE), mean absolute percentage error (MAPE) and mean absolute error (MAE) to
323 quantify the uncertainty of new model. We use the coefficient of determination R^2 to describe the
324 goodness of fit between the model-derived data series and the measured data. Accordingly, our
325 model had an R^2 value of approximately 0.98, indicating a strong correlation between observed and
326 predicted lake water storages (Figure 8). Moreover, our model has the lowest variance, according
327 to a bias (-0.0031 km³), MAE (0.0059 km³), RMSE (0.0096 km³), and MAPE(25%). Also, our
328 model has the lowest average relative error, at around 14%. The average relative error of EqS2,
329 EqS3, EqS5, EqS7, EqS9, EqS11, EqS15 and EqS16 ranged from 44% to 50%, while the remaining
330 formulas display average relative errors exceeding 50%. Although all equations achieved $R^2 > 0.93$,
331 the predicted values have a high variance and tend to either overestimate or underestimate the water
332 storage of glacial lakes. Compared with our method, their bias, MAE, RMSE, and MAPE were all
333 55%, 64%, 52% and 64%, respectively, and thus higher than ours. EqS7 had a better prediction
334 accuracy. However, its bias, MAE and RMSE values are 82%, 64% and 52% higher than those of
335 our model, respectively. This indicates a significant estimation error for specific glacial lakes, and
336 both RMSE and MAE are sensitive to outliers. Overall, most of the equations tend to underestimate
337 glacial lake water storages, with the underestimation becoming more pronounced for larger water
338 storages. Nevertheless, we consider the accuracy level of our method to be acceptable due to the
339 lower uncertainty compared to other models, providing an alternative for predicting the water
340 storage of MDLs.



341

342 **Figure 8.** Comparison of the overall performance in glacial lake water storage estimation between our and

343 previous models (a) and comparison of measured and estimated water storage by our model (b).

344

345 **Table 6** Comparison of all empirical scaling relationships (EqS1-EqS20) in terms of bias, mean absolute error (MAE)

346 and root mean square error (RMSE) are measured in cubic kilometers. See Appendix B for details.

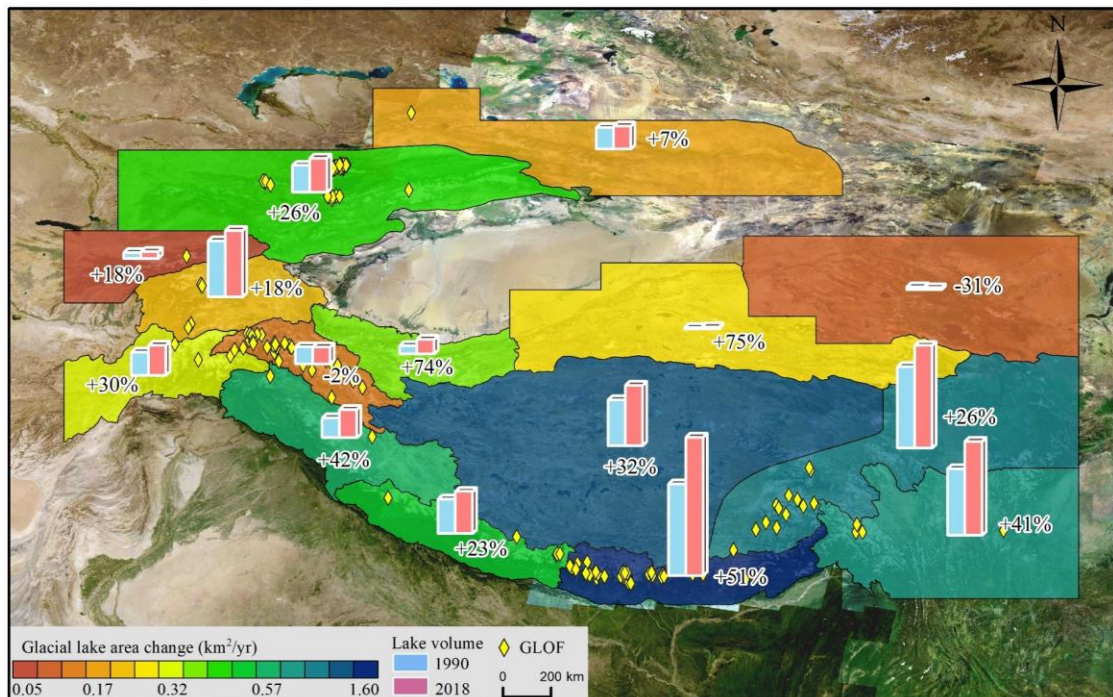
Equation	RE	BIAS	MAE	MAPE	R ²	RMSE
Our model	14%	-0.0031	0.0059	25%	0.9793	0.0096
Zhou et al., 2021	53%	0.0097	0.0142	95%	0.9289	0.0485
Eq1	63%	-0.0060	0.0104	49%	0.9654	0.0174
Eq2	49%	-0.0185	0.0192	130%	0.9521	0.0299
Eq3	50%	-0.0074	0.0100	44%	0.9556	0.0150
Eq4	164%	0.0448	0.0448	120%	0.9494	0.1035
Eq5	45%	-0.0056	0.0112	51%	0.9418	0.0182
Eq6	219%	0.0609	0.0609	130%	0.9509	0.1331
Eq7	48%	-0.0056	0.0097	41%	0.9516	0.0146
Eq8	52%	-0.0162	0.0177	117%	0.9621	0.0295
Eq9	49%	-0.0126	0.0143	74%	0.9556	0.0213
Eq10	50%	-0.0149	0.0164	98%	0.9596	0.0262
Eq11	49%	-0.0112	0.0131	63%	0.9551	0.0192
Eq12	94%	0.0089	0.0118	37%	0.9642	0.0186
Eq13	853%	0.2362	0.2362	159%	0.9590	0.4404
Eq14	51%	0.0022	0.0113	61%	0.9438	0.0268
Eq15	46%	-0.0048	0.0110	50%	0.9430	0.0182
Eq16	44%	-0.0153	0.0160	88%	0.9288	0.0230
Eq17	316%	0.2088	0.2089	292%	0.8736	0.7300
Eq18	77%	0.0178	0.0207	98%	0.9418	0.0582
Eq19	50%	0.0036	0.0124	74%	0.9379	0.0336

Eq20	132%	0.000238	0.0132	59%	0.9501	0.0245
------	------	----------	--------	-----	--------	--------

347 **4.3. Application of the new model**

348 Considering the frequent occurrence of GLOF events in High Mountain Asia, posing threats to
 349 downstream infrastructure and the safety of the lives and properties of the local communities,
 350 assessing the water storage of glacial lakes is crucial for management potentially hazardous ones
 351 (Nie et al., 2023). Therefore, this study employs our model to provide preliminary estimates of
 352 glacial lake water storages in the study area.

353 A glacial lake inventory data (Wang et al., 2020) reveals that in 2018, there were a total of
 354 13,166 glacial lakes ($\geq 0.01 \text{ km}^2$) distributed in High Mountain Asia. The dataset highlights a
 355 significant increase in both the number and area of GCLs from 1990 to 2018, experiencing a
 356 remarkable growth of 52% and 54%, respectively. Model estimation results indicate that the total
 357 glacial lake water storage in the study area was 37.18 km^3 in 2018. Over the past three decades, the
 358 overall MDL's water storage increased by 8.94 km^3 from 28.24 km^3 in 1990, representing a growth
 359 of approximately 32%. The expansion rates of glacial lakes varied significantly across different
 360 regions (Figure 9). Notably, the Hindu Kush-Karakoram and the central and eastern of the
 361 Himalayas to the Hengduan Mountains witnessed the fastest increases in both glacial lake area and
 362 water storage.



363

364 **Figure 9** Changes in the area and water storage of glacial lakes from 1990 to 2018 in High Mountain Asia. The base

365 map is a Google Earth image (©Google Earth).

366 The Eastern Himalayas had the largest gain in both the area and water storage of glacial lakes,
367 concurrently establishing it as a hotspot for frequent GLOFs (Figure 9). The results indicate that the
368 water storage of 1,410 MDLs ($\geq 0.01 \text{ km}^2$) within the study area was $9,337 \pm 990 \times 10^6 \text{ m}^3$ in 2022.
369 Among these, GCLs and GULs account for 70% and 30% of the total water storage, respectively.
370 Between 1990 and 2022, the total water storage in glacial lakes representing a substantial growth of
371 162%. Notably, GCLs contributed 134% with an average annual growth rate of $8.8\% \text{ a}^{-1}$, indicating
372 an overall increase of 280%. In contrast, the change in the water storage of unconnected lakes
373 remained relatively stable, experiencing a modest growth of 52% over the past 32 years,
374 considerably lower than that of GCLs.

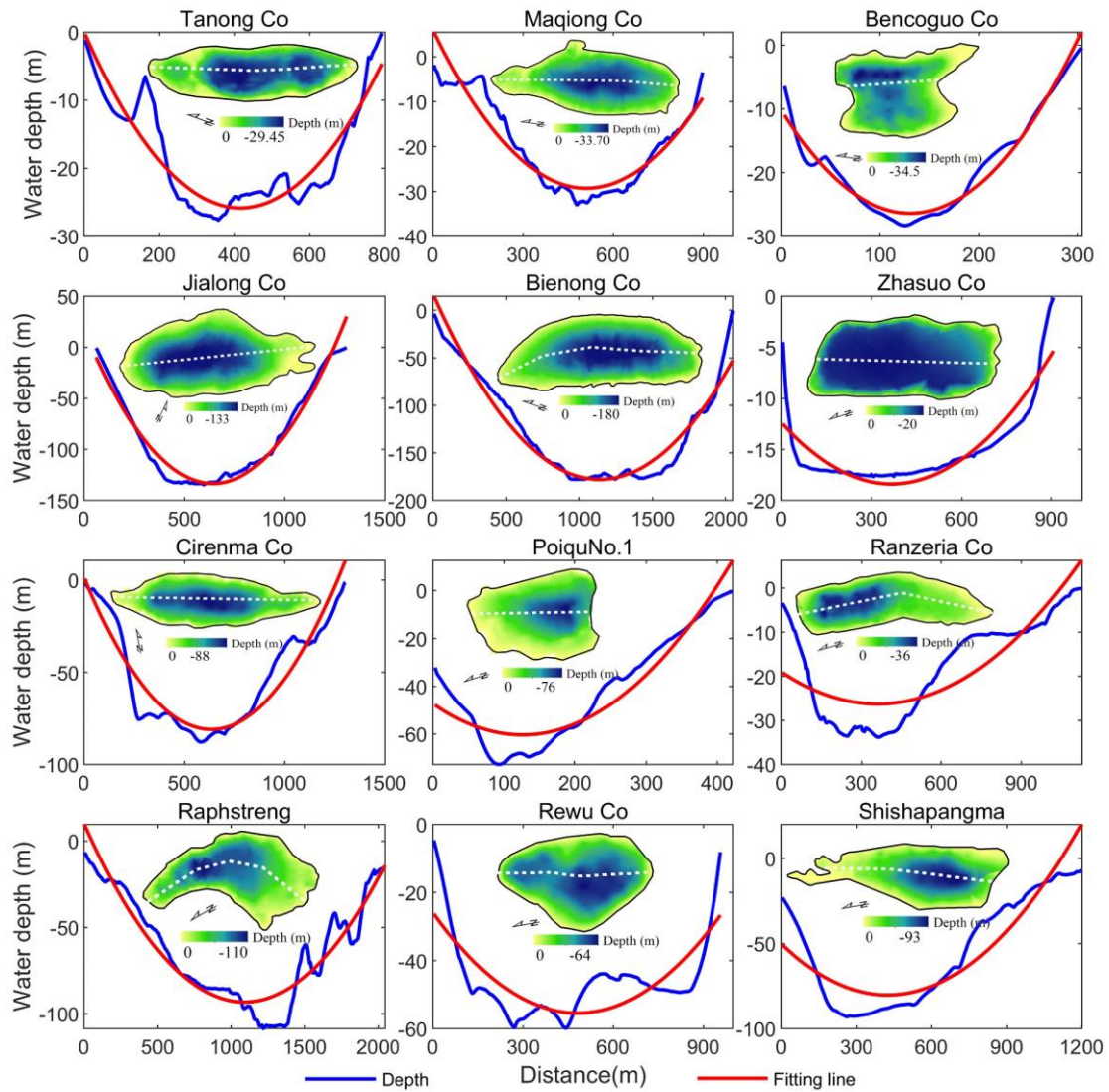
375 **5. Discussion**

376 **5.1 Justification and uncertainty of model assumptions**

377 In this study, we discuss the rationality and uncertainty of the model from three aspects. We
378 first assumed that the MDL features a parabolic longitudinal bottom profile and a uniformly
379 distributed sediment layer. The basin morphology of glacial lakes is a result of glacial erosion during
380 the glacier retreat process. Glacier erosion involves certain lateral shear stress, leading to the
381 formation of U-shaped valleys. Glacial lakes develop on these U-shaped valley terrains (Seddik et
382 al., 2009). Therefore, based on the lake bathymetry and the longitudinal bottom profile of the MDLs
383 (Figure 10), the variations in the underwater morphology of MDLs can be fitted with a parabolic
384 curve. However, when observing trends in underwater topography, it is evident that some large and
385 deep lakes (depth $> 100 \text{ m}$), such as Jialong Co and Bienong Co, exhibit relatively flat underwater
386 terrain, while others do not (Figure 7). This finding aligns with the research conducted by Carrivick
387 and Tweed (2013), who proposed that most proglacial lake basins have flat landforms resulting from
388 extensive sedimentation. These flat terrains, which were previously subdued and smoothed by
389 glaciation, can become covered and obscured by thin layers of silts and clays. Furthermore, it has
390 been suggested by some scholars that in large and deep proglacial lakes, the instability of the glacier
391 margin and the increased likelihood of wave erosion can lead to the erosion of moraine ridges at the
392 lake bottom (Murton et al., 2012).

393 The underwater landforms of some MDLs are not always a smooth parabolic shape. As
394 depicted in Figure 11, the bottom topography of most glacial lakes exhibits a fluctuating parabolic

395 trend. Golledge (2008) and Bennett et al. (2000) revealed that subaqueous moraines in glacial lakes
 396 often have linear or sinuous crests, and their ridges frequently exhibit heavily glactectonized
 397 sediment structures indicative of compression. Although the presence of subaqueous moraines is
 398 uncertain, this perspective offers a plausible explanation for the fluctuations in underwater
 399 topography. In conclusion, concerning the formation process of subglacial geomorphology in MDLs
 400 and lake bathymetry, both aspects substantiate our postulation that the MDL features a parabolic
 401 longitudinal bottom profile. Furthermore, we hypothesize the presence of uniform sediment surface
 402 to keep $h_1 = h_2$, although sediment distribution may be non-uniform due to factors such as the
 403 position of the ice margin and water density (Carrivick and Tweed, 2013). As a result, the uneven
 404 terrain at the bottom of some glacial lakes or the non-uniform distribution of sediments therein
 405 constitutes one of the sources of uncertainty in the model.



406
 407 **Figure 10.** The longitudinal bottom profile underwater topography of the MDLs obtained by bathymetry and the

408 fitting lines of terrain change trend (The white dotted line is the longitudinal profile line of the lake).

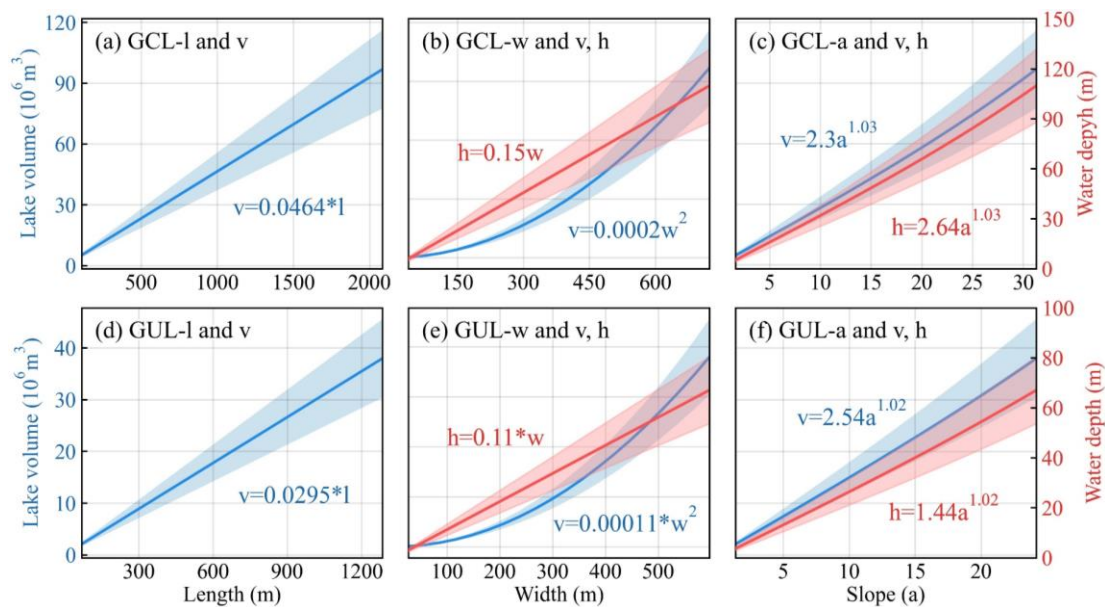
409 The second source of uncertainty in the model arises from the assumption regarding the lake
410 surface of the MDL. Here, we assumed MDL's surface shape is characterized by an ellipse at both
411 ends and a rectangle in between. MDLs develop on parabolic or U-shaped glacial troughs. A mature
412 MDL, characterized by a relatively stable surface morphology, tends to exhibit an elliptical shape
413 due to its geological characteristics (e.g., GUL lake type in Figure 5). Similar trends in the
414 boundaries of MDLs are observed in different lake catalog datasets. Furthermore, in this study,
415 MDLs are classified into four types based on their geometric shapes (see Table 1). Treating the
416 complete geometric shape of an MDL as an ellipse allows the model to automatically partition the
417 lake basin structure (e.g., V_1 , V_2 , V_3 in Figure 2) based on the lake's shape coefficient, facilitating
418 the calculation of the water storage for MDLs with different morphologies. However, in reality, as
419 suggested by Teller (1987) and Rubensdotter et al. (2009), factors such as the position of the glacier
420 margin, surrounding landscape elevation and topography, and the location and elevation of lake
421 overflow channels can affect the basin morphology of MDLs. For instance, Bencoguo Co and
422 Raphstreng in Figure 10 do not exhibit the characteristic elliptical shape on the lake surface. This
423 uncertainty in the geometric shape of the lakes may lead to an overestimation of lake water storage
424 in the model, as the maximum width of the lake significantly influences the model results.

425 Finally, assuming the slope angle near the lake remains constant ($\alpha=\beta$) is another aspect
426 contributing to the uncertainty in the model. In actuality, the slopes surrounding the lake exhibit
427 variations influenced by factors like the glacier tongue's position, the surrounding topography, and
428 the presence of moraine ridges. This variability in slope angles can further contribute to the
429 uncertainty when estimating the model's maximum water depth and water storage.

430 5.2 Sensitivity of model input parameters

431 Additionally, our model requires key parameters, namely, w , l , a , m , n , and r , with the
432 relationship between m , n , r , and l defined as $l = m + n + r$. Thus, we only investigated the sensitivity
433 of our model to l , w , and a . Since water depth is closely related to w and a (see equation (13)), we
434 also conducted parameter sensitivity tests on the estimated water depth using our model. In this
435 study, we employed Jialong Co and Bienong Co as representatives of GUL and GCL of MDLs,
436 respectively, to assess the sensitivity of the model to various parameters across different types of
437 glacial lakes. Figure 11 (a-f) demonstrates the sensitivity of volume (v) and water depth (h) in our

438 model to variations in the maximum length (l), maximum width (w), and slope (a) of glacial lakes.
 439 Overall, there was a linear increase in glacial lake volume with changes in length (Figures 11a and
 440 d). As shown in Figures 11b and e, variations in maximum width exhibited a consistent power-law
 441 relationship with volume, where volume increased exponentially with width. The water depth of
 442 glacial lakes demonstrated a linear increase with changes in width. The slope of the lake's edge
 443 showed a power-law relationship with both estimated water depth and volume (Figures 11e and f).
 444 In summary, when estimating volume using our model, glacial lake width and slope were found to
 445 be the most sensitive parameters, followed by the lake's length. Regarding water depth, the model
 446 was most sensitive to the slope, followed by the width.



447
 448 **Figure 11.** Parameter sensitivity analysis for glacial lake volume estimation using new model (note: the shaded
 449 part represents the confidence interval, and definition of parameters in the figure as shown in Table 2).

450 6. Conclusion

451 Water storage plays a crucial role in predicting peak discharge of GLOFs. This study proposed
 452 a mathematically robust and cost-effective approach for estimating lake water storage in regions
 453 where field measurements of bathymetry are limited. The new model utilized lake geometry and
 454 DEMs to estimate lake water storage. By parameterizing the model based on assumptions such as a
 455 parabolic longitudinal bottom profile and consistent slope angles, it offers a reliable estimation of
 456 lake water storage.

457 We validated our parameterization using bathymetry measurements from four representative
 458 glacial lakes, namely, Bienong Co, Maqiong Co, Tanong Co, and Jialong Co, located in the Qinghai-

459 Tibet Plateau. Additionally, we applied the new model to 10 glacial lakes with depth measurements
460 conducted during 2020-2021, and we included bathymetry data from 34 other glacial lakes sourced
461 from published literature. Our model overcomes the autocorrelation issue inherent in earlier
462 area/depth-water storage relationships and incorporates an automated calculation process based on
463 the topography and geometrical parameters specific to MDLs. Compared to other models, our model
464 achieved the lowest average relative error of approximately 14% when analyzing 44 observed data,
465 surpassing the >44% average relative error from alternative models. This study model will allow
466 researchers and practitioners to better predict potential outburst water storages and peak discharge
467 of MDLs.

468 **Competing interests**

469 The contact author has declared that none of the authors has any competing interests.

470 **Data availability**

471 All data used in this study can be found in Table 5 and supplementary files.

472 **Acknowledgments**

473 This work was supported by research grants from the Second Tibetan Plateau Scientific Expedition
474 and Research (STEP, Grant No. 2019QZKK0208), the National Key Research and Development
475 Program of China (No. 2021YFE0116800), the postdoctoral research start-up project of Yunnan
476 Normal University (Grant No. 01300205020503329), the National Natural Science Foundation of
477 China (No. 42171129, 42301154).

478 **References:**

- 479 Bennett, M.R., Huddart, D., McCormick, T., 2000. The glaciolacustrine landform–sediment
480 assemblage at Heinabergsjökull, Iceland. *Geografiska Annaler: Series A, Physical Geography*,
481 82(1), 1-16.
- 482 Bolch, T., Kulkarni, A., Käab, A., Huggel, C., Paul, F., Cogley, J. G., Frey, H., Kargel, J. S., Fujita,
483 K., Scheel, M., Bajracharya, S., Stoffel, M., 2012. The state and fate of Himalayan glaciers.
484 *Science*, 336(6079), 310-314.
- 485 Carrivick, J.L., Quincey, D.J., 2014. Progressive increase in number and water storage of ice-
486 marginal lakes on the western margin of the Greenland Ice Sheet. *Global and Planetary Change*,
487 116, 156-163.
- 488 Carrivick, J.L., Tweed, F.S., 2013. Proglacial lakes: character, behaviour and geological importance.

489 Quaternary Science Reviews, 78, 34-52.

490 Clague, J.J., Evans, S.G., 2000. A review of catastrophic drainage of moraine-dammed lakes in
491 British Columbia. *Quaternary Science Reviews*, 19(17-18), 3-1783.

492 Cook, K.L., Andermann, C., Gimbert, F., Adhikari, B.R., Hovius, N., 2018. Glacial lake outburst
493 floods as drivers of fluvial erosion in the Himalaya. *Science*, 362(6410), 53-57.

494 Cook, S.J., Quincey, D. J., 2015. Estimating the water storage of Alpine glacial lakes. *Earth Surface
495 Dynamics*, 3(4), 559-575.

496 Duan, H., Yao, X., Zhang, Y., Jin, H., Wang, Q., Du, Z., Hu, J., Wang, B., Wang, Q., 2023. Lake
497 water storage and potential hazards of moraine-dammed glacial lakes—a case study of Bienong
498 Co, southeastern Tibetan Plateau. *The Cryosphere*, 17(2), 591-616.

499 Emmer, A. and Vilímek, V.: New method for assessing the susceptibility of glacial lakes to outburst
500 floods in the Cordillera Blanca, Peru, *Hydrol. Earth Syst. Sci.*, 18, 3461–3479,
501 <https://doi.org/10.5194/hess-18-3461-2014>, 2014.

502 Fischer, M., Korup, O., Veh, G., Walz, A. 2021. Controls of outbursts of moraine-dammed lakes in
503 the greater Himalayan region. *The Cryosphere*, 15(8), 4145-4163.

504 Fujita, K., Sakai, A., Takenaka, S., Nuimura, T., Surazakov, A. B., Sawagaki, T., & Yamanokuchi,
505 T., 2013. Potential flood water storage of Himalayan glacial lakes. *Natural Hazards and Earth
506 System Sciences*, 13(7), 1827-1839.

507 Gao, Y., Liu, S., Qi, M., Xie, F., Wu, K., Zhu, Y., 2021. Glacier-related hazards along the
508 International Karakoram Highway: status and future perspectives. *Frontiers in Earth Science*,
509 9, 611501.

510 Golledge, N.R., Phillips, E., 2008. Sedimentology and architecture of De Geer moraines in the
511 western Scottish Highlands, and implications for grounding-line glacier dynamics.
512 *Sedimentary Geology*, 208(1-2), 1-14.

513 Harrison, S., Kargel, J.S., Huggel, C., Reynolds, J., Shugar, D.H., Betts, R.A., Emmer, A., Glasser,
514 N., Haritashya, U.K., Klimeš, J., Reinhardt, L., 2021. Climate change and the global pattern of
515 moraine-dammed glacial lake outburst floods. *The Cryosphere*, 12(4), 1195–1209.

516 Liermann, S., Beylich, A. A., van Welden, A., 2012. Contemporary suspended sediment transfer and
517 accumulation processes in the small proglacial Sætrevatnet sub-catchment, Bødalen, western
518 Norway. *Geomorphology*, 167, 91-101.

519 Liu, S., Wu, T., Wang, X., Wu, X., Yao, X., Liu, Q., Zhang, Y., Wei, J., Zhu, X., 2021. Changes in
520 the global cryosphere and their impacts: A review and new perspective. *Sciences in Cold and*
521 *Arid Regions*, 12(6), 343-354.

522 Lützow, N., Veh, G., Korup, O., 2023. A global database of historic glacier lake outburst floods.
523 *Earth System Science Data Discussions*, 15(7), 2983–3000.

524 Mergili, M., Pudasaini, S. P., Emmer, A., Fischer, J.-T., Cochachin, A., and Frey, H.: Reconstruction
525 of the 1941 GLOF process chain at Lake Palcacocha (Cordillera Blanca, Peru), *Hydrol. Earth*
526 *Syst. Sci.*, 24, 93–114, <https://doi.org/10.5194/hess-24-93-2020>, 2020.

527 Murton, D.K., & Murton, J.B., 2012. Middle and Late Pleistocene glacial lakes of lowland Britain
528 and the southern North Sea Basin. *Quaternary International*, 260, 115-142.

529 Nie, Y., Deng, Q., Pritchard, H. D., Carrivick, J.L., Ahmed, F., Huggel, C., Liu, L., Wang, W., Lesi,
530 M., Wang, J., Zhang, H., Zhang, B., Lü, Q., Zhang, Y., 2023. Glacial lake outburst floods
531 threaten Asia's infrastructure. *Science bulletin*, 68 (13), 1361-1365.

532 Patel, L.K., Sharma, P., Laluraj, C., Thamban, M., Singh, A., Ravindra, R., 2017. A geospatial
533 analysis of Samudra Tapu and Gepang Gath glacial lakes in the Chandra Basin, Western
534 Himalaya. *Nat. Hazards* 86, 1275–1290.

535 Qi, M., Liu, S., Wu, K., Zhu, Y., Xie, F.M., Jing, H.A., Gao, Y.P., Yao, X.J., 2022. Improving the
536 accuracy of glacial lake water storage estimation: a case study in the Poiqu basin, central
537 Himalayas. *Journal of Hydrology*, 610, 127973.

538 Richardson, S.D., Reynolds, J.M., 2000. An overview of glacial hazards in the Himalayas.
539 *Quaternary International*, 65, 31-47.

540 Rounce, D.R., Hock, R., Maussion, F., Hugonnet, R., Kochtitzky, W., Huss, M., Berthier, E.,
541 Brinkerhoff, D., Compagno, L., Copland, L., Farinotti, D., Menounos, B., McNabb, R. W.,
542 2023. Global glacier change in the 21st century: Every increase in temperature matters. *Science*,
543 379(6627), 78-83.

544 Rubensdotter, L., Rosqvist, G., 2009. Influence of geomorphological setting, fluvial-, glaciofluvial-
545 and mass-movement processes on sedimentation in alpine lakes. *The Holocene*, 19(4), 665-
546 678.

547 Sattar, A., Haritashya, U.K., Kargel, J.S., Leonard, G.J., Shugar, D.H., Chase, D.V. 2021., Modeling
548 lake outburst and downstream hazard assessment of the Lower Barun Glacial Lake, Nepal

549 Himalaya. *Journal of Hydrology*, 598, 126208.

550 Seddik, H., Greve, R., Sugiyama, S., Naruse, R., 2009. Numerical simulation of the evolution of
551 glacial valley cross sections. arXiv preprint arXiv:0901.1177.

552 Shugar, D.H., Burr, A., Haritashya, U.K., Kargel, J.S., Watson, C.S., Kennedy, M.C., Bevington,
553 A.R., Betts, R.A., Harrison, S., Strattman, K., 2020. Rapid worldwide growth of glacial lakes
554 since 1990. *Nature Climate Change*, 10(10), 939-945.

555 Teller, J. T., 1987. Proglacial lakes and the southern margin of the Laurentide Ice Sheet. In:
556 Ruddiman, W.F., Wright, H.E. (Eds.), *North America and Adjacent Oceans During the Last*
557 *Deglaciation. The Decade of North American Geology*. Geological Society of America,
558 Boulder, CO, K3, pp. 39–69.

559 Veh G , Korup O , Walz A .Hazard from Himalayan Glacier Lake Outburst Floods[J].*Proceedings*
560 *of the National Academy of Sciences*, 2019, 117(2).DOI:10.1073/pnas.1914898117.

561 Veh, G., Korup, O., von Specht, S., Roessner, S., Walz, A., 2019. Unchanged frequency of moraine-
562 dammed glacial lake outburst floods in the Himalaya. *Nature Climate Change*, 9(5), 379-383.

563 Veh, G., Lützwow, N., Kharlamova, V., Petrakov, D., Hugonnet, R., Korup, O., 2022. Trends, breaks,
564 and biases in the frequency of reported glacier lake outburst floods. *Earth's Future*, 10(3),
565 e2021EF002426.

566 Wang, W., Gao, Y., Anacona, P.I., Lei, Y., Xiang, Y., Zhang, G., Li, S., Lu, A., 2018. Integrated
567 hazard assessment of Cirenmaco glacial lake in Zhangzangbo valley, Central Himalayas.
568 *Geomorphology*, 306, 292-305.

569 Wang, X., Guo, X., Yang, C., Liu, Q., Wei, J., Zhang, Y., Liu, S., Zhang, Y., Jiang, Z., Tang, Z., 2020.
570 Glacial lake inventory of high-mountain Asia in 1990 and 2018 derived from Landsat images.
571 *Earth System Science Data*, 12(3), 2169-2182.

572 Westoby, M.J., Glasser, N.F., Brasington, J., Hambrey, M.J., Quincey, D.J., Reynolds, J.M., 2014.
573 Modelling outburst floods from moraine-dammed glacial lakes. *Earth-Science Reviews*, 134,
574 137-159.

575 Wu, G., Yao, T., Wang, W., Zhao, H., Yang, W., Zhang, G., Li, S., Yu, W., Lei, Y., Hu, W. 2019.,
576 Glacial hazards on Tibetan Plateau and surrounding alpine. *Bulletin of Chinese Academy of*
577 *Sciences (Chinese Version)*, 34(11), 1285-1292.

578 Zhang, G., T. Bolch, T. Yao, D.R. Rounce, W. Chen, G. Veh, O. King, S.K. Allen, M. Wang, W.W.,

579 2023. Underestimated mass loss from lake-terminating glaciers in the greater Himalaya. *Nature*
580 *Geoscience*. 16, 333–338.

581 Zheng, G., Allen, S. K., Bao, A., Ballesteros-Cánovas, J.A., Huss, M., Zhang, G., Li, J., Yuan, Y.,
582 Jiang, L., Yu, T., Chen, W., Stoffel, M., 2021a. Increasing risk of glacial lake outburst floods
583 from future Third Pole deglaciation. *Nature Climate Change*, 11(5), 411-417.

584 Zheng, G., Mergili, M., Emmer, A., Allen, S., Bao, A., Guo, H., Stoffel, M., 2021. The 2020 glacial
585 lake outburst flood at Jinwuco, Tibet: causes, impacts, and implications for hazard and risk
586 assessment. *The Cryosphere*, 15(7), 3159-3180.

587 Zhou, L.X., Liu, J.K., Li, Y.L., 2020. Calculation method of mathematical model of the moraine
588 dammed lake storage capacity. *Sci. Technol. Eng*, 20, 9804-9809.

589 Zhu, S., Liu, B., Wan, W., Xie, H., Fang, Y., Chen, X., Hong, Y., 2019. A new digital lake bathymetry
590 model using the step-wise water recession method to generate 3D lake bathymetric maps based
591 on DEMs. *Water*, 11(6), 1151.